

See discussions, stats, and author profiles for this publication at: <http://www.researchgate.net/publication/287122746>

# Silicon Carbide-based Membranes with High Soot Particle Filtration Efficiency, Durability and Catalytic Activity for CO/HC Oxidation and Soot Combustion

ARTICLE *in* JOURNAL OF MEMBRANE SCIENCE · DECEMBER 2015

Impact Factor: 5.06 · DOI: 10.1016/j.memsci.2015.12.015

---

READS

8

10 AUTHORS, INCLUDING:



[P. Vernoux](#)

French National Centre for Scientific Resea...

153 PUBLICATIONS 1,357 CITATIONS

[SEE PROFILE](#)



[Corneliu Balan](#)

Polytechnic University of Bucharest

56 PUBLICATIONS 452 CITATIONS

[SEE PROFILE](#)



[Philippe Miele](#)

Ecole Nationale Supérieure de Chimie de M...

285 PUBLICATIONS 4,142 CITATIONS

[SEE PROFILE](#)



[Samuel Bernard](#)

Université de Montpellier

109 PUBLICATIONS 1,209 CITATIONS

[SEE PROFILE](#)



ELSEVIER

Contents lists available at ScienceDirect

## Journal of Membrane Science

journal homepage: [www.elsevier.com/locate/memsci](http://www.elsevier.com/locate/memsci)

# Silicon carbide-based membranes with high soot particle filtration efficiency, durability and catalytic activity for CO/HC oxidation and soot combustion



Fabien Sandra<sup>a</sup>, Anthony Ballesterio<sup>a</sup>, Van Lam NGuyen<sup>b</sup>, Michail N. Tsampas<sup>c</sup>,  
Philippe Vernoux<sup>c</sup>, Corneliu Balan<sup>d</sup>, Yuji Iwamoto<sup>e</sup>, Umit B Demirci<sup>a</sup>, Philippe Miele<sup>a</sup>,  
Samuel Bernard<sup>a,\*</sup>

<sup>a</sup> IEM (Institut Européen des Membranes), UMR 5635 (CNRS-ENSCM-UM), Université Montpellier, Place E. Bataillon, F- 34095 Montpellier, France

<sup>b</sup> Dipartimento di Ingegneria Industriale, Università di Trento, Via Sommarive 9, Trento 38123, Italy; Present address: IEM (Institut Européen des Membranes), UMR 5635 (CNRS-ENSCM-UM), Université Montpellier, Place E. Bataillon, F-34095 Montpellier, France

<sup>c</sup> Université Lyon 1, CNRS, UMR 5256, IRCELYON, Institut de Recherches sur la Catalyse et l'Environnement de Lyon, 2 avenue Albert Einstein, F-69626 Villeurbanne, France

<sup>d</sup> REOROM Laboratory, Hydraulics Department, University "Politehnica" of Bucharest, Splaiul Independentei 313, 060042 Bucharest, Romania

<sup>e</sup> Nagoya Inst Technol, Grad Sch Engr, Dept Frontier Mat, Showa Ku, Nagoya, Aichi 4668555, Japan

## ARTICLE INFO

## Article history:

Received 13 August 2015

Received in revised form

4 November 2015

Accepted 5 December 2015

Available online 9 December 2015

## Keywords:

Silicon carbide

Membranes

Diesel particulate filter

Ceria-based catalysts

Soot combustion

## ABSTRACT

We report here the solution coatings of Diesel Particulate Filter (DPF) with allylhydridopolycarbosilane (AHPCS)-based polymers leading to supported silicon carbide (SiC)-based membranes with high temperature soot particle filtration efficiency, durability and catalytic activity. In a first part of the present study, our objective was to reduce the pore size of DPF to filtrate finer particles without altering filtration efficiency by coating DPF with an additional fine porous AHPCS-derived SiC membrane. The latter is produced by dip-coating AHPCS on DPF following by a pyrolysis of the AHPCS membrane-modified DPF at 1000 °C under argon. We investigated the influence of dip-coating parameters and viscosity of different AHPCS solutions on the SiC membrane-coated DPF by SEM, mercury porosimetry, XRD and high-temperature thermogravimetric analysis. The evolution of the filtration capacity has been determined with a synthetic gas bench. An additional fine SiC membrane (~150 nm in thickness) prepared from a 10 vol% of AHPCS in THF deposited on DPF allowed maintaining filtration efficiency as high as the virgin DPF while the pore size of the SiC membrane coated-DPF decreased to filter finer particles. Results are confirmed using a commercially-available polysiloxane (Si–C–O precursor). Furthermore, the SiC membrane acted as a thermal barrier coating and provided a better durability to the DPF by preventing apparition of cracks after heat-treatment to 1500 °C under argon. The use of mixed oxide and metallic phases formed *in-situ* in SiC constitutes one of the solutions to generate new and effective catalytic performances to membranes. Within this context, in a second part of the study, we applied a reverse AHPCS-based microemulsion to combine SiC and oxide phases in the same additional porous membrane. As a proof of concept, we have prepared catalytically active Ce–O–Fe–Pt/SiC membrane coated DPF after dip-coating and pyrolysis under argon. These materials have been characterized and tested with regard to CO/HC oxidation and soot combustion. Ce–O–Fe–Pt/SiC membrane coated DPF showed an activity for CO conversion reaching a light-off temperature  $T_{50}=270$  °C and the presence of the catalytic phase allowed burning soot at 486 °C.

© 2015 Elsevier B.V. All rights reserved.

## 1. Introduction

Recently, the impact of technical membrane technology has exponentially increased in research settings and industrial applications mainly due to the chemical and petrochemical industries

[1]. A technical membrane can be defined as a barrier that permits selective mass transport between two phases [2]. It is selective because some components can pass the membrane more easily than others according to their porosity. Technical membranes offer nowadays the greatest industrial potential in fluid separation technologies in terms of low capital investment, overall energy savings, low weight, required facility foot-print, space requirement

\* Corresponding author.

and high process flexibility [3].

The exhaust emissions from Diesel engines include important contaminants, nitrogen oxides ( $\text{NO}_x$ ), carbon monoxide (CO) with a significant level of particulate matter (PM) that consists mostly of carbonaceous soot and soluble hydrocarbons (HC) condensed on the soot [4,5]. Since 2009 and the 'Euro 5' standard, Diesel cars have required fitment of a Diesel Particulate Filter (DPF) to filtrate the contaminants [6]. It represents a honeycomb monolith, usually made of silicon carbide (SiC) which is now considered as a state-of-the-art system for the safe and effective reduction of Diesel engine exhaust gases.

The constant filtration of the exhaust gases generates a progressive accumulation of soot which requires the filter regeneration by combustion of the retained soot [7,8]. Active regeneration of the DPFs involves fuel post-injection, which is used for increasing the exhaust temperature up to the soot ignition, via exothermic oxidations of unburnt hydrocarbons in the Diesel Oxidation Catalyst (DOC) placed up-stream the DPF. To limit the fuel overconsumption induced by post-injections, catalysts are either added in the combustion chamber as liquid additives [9–11] or deposited in the DPF channels by solution combustion synthesis [12], impregnation [13], washcoating [14] and combination methods [15]. A large number of catalyst formulations have been reported for soot combustion. Cerium-based compounds have been mainly investigated as the catalytically active phases because of their ability to release and store oxygen [16–20].

Due to the tighter emission standards, the demand for more energy efficient vehicles and the severe operating conditions of the exhausts pipe such as high flows, high corrosive atmospheres, thermal shocks and vibrations, it is essential to have future developments of particle filters. One of the most desirable ways for increasing the filtration efficiency (future emission standards) would be to use an additional fine porous filtration membrane (=coating) on the filter wall. Preferentially, the composition of this membrane would be SiC to match the thermal expansion coefficient of DPF and satisfy the severe operating conditions. In addition, the SiC membrane is expected to display high temperature catalytic activity in order to offer in the same materials both soot particulate filtration efficiency, durability and activity for CO/HC oxidation and soot combustion. This is the double objective we have fixed in our study: on the one hand, the feasibility to coat a commercial lab-scale DPF with a thin SiC membrane and on the other hand to render catalytically active this membrane using ceria-based catalysts formed *in-situ* during the SiC membrane elaboration.

The manufacturing process of SiC was initiated by Acheson in 1892 [21,22] and is still today applied to produce the commercially available SiC ( $\alpha$ -SiC). This process is not adapted to the preparation of fine porous filtration membrane coatings and does not allow to generate *in-situ* the catalytic phase within the SiC matrix. Chemistry is clearly the way to achieve this goal. Gas phase coating methods allow producing thin non-oxide ceramic coatings [23,24]. However, such processes are relatively expensive and time consuming and the generation of single or mixed oxide and metallic phases in the SiC matrix is extremely complex to achieve. Liquid phase coating methods are more appropriate. An easy approach is the Polymer-Derived Ceramics (PDCs) route [25–40].

The PDCs route is making an increasingly important contribution to the research development and manufacture of non-oxide ceramics from preceramic polymers and may find many applications in environment [38] and energy [39,40]. The processing of coatings based on the PDCs route can be divided into three steps: 1) Synthesis of a preceramic polymer; 2) dip-coating followed by cross-linking of the precursor into an infusible network; 3) conversion into ceramic coatings by pyrolysis [41–47].

In polymer-derived SiC, amorphous structures are formed at relatively low temperature (800–1000 °C). They exhibit atomically

homogenous elemental distributions and they have demonstrated excellent creep, corrosion, chemical, and oxidation resistance [34]. These properties are complimented by temperature stability of the amorphous network. Novel properties are also expected to emerge through the modification of the SiC precursor with other low molecular weight precursors leading to the precipitation of secondary phases inside the PDC matrix during the pyrolysis [25–31,48–51].

Herein, we investigate the PDCs route using organosilicon precursors to coat DPF with an additional SiC-based membrane. Supported SiC membranes have been already developed for  $\text{H}_2$  permselectivity [52–57]. To our knowledge, SiC membranes coated on DPF have never been reported for high temperature soot particle filtration efficiency. Here, the materials are prepared from organosilicon polymers (allylhydridopolycarbosilane (AHPCS), SiC precursor [58,59]) by dip-coating and pyrolysis. Complete characterization is done at different length scales using complementary characterization tools. It is demonstrated, by means of reproducible soot loading experiments on a special laboratory test bench, that the additional fine porous SiC membrane (~150 nm in thickness) allowed decreasing the pore size diameter of DPF to filter fine particles without altering filtration efficiency while improving the durability at high temperature in comparison to the virgin DPF.

Combining filtration efficiency, durability and catalytic activity in a same membrane is a great challenge. To reach this objective, we investigated as a proof of concept a microemulsion method coupled with the PDCs route.

Microemulsions are isotropic, macroscopically homogeneous, and thermodynamically stable solutions containing at least three components, namely a polar phase (usually water), a nonpolar phase (usually oil) and a surfactant. On a microscopic level the surfactant molecules form an interfacial film separating the polar and the non-polar domains. This interfacial layer forms three basic types of microemulsions ranging from droplets of oil dispersed in a continuous water phase (O/W-direct microemulsion) over a bi-continuous phase to water droplets dispersed in a continuous oil phase (W/O-reverse microemulsion). Depending on the proportion of various components and the hydrophilic-lipophilic balance value of the surfactant used, the formation of microdroplets can be in the form of oil-swollen micelles dispersed in water as oil-in-water (O/W) microemulsion or water swollen micelles dispersed in oil as for water-in-oil (W/O) microemulsion, also called reverse microemulsion. Here, a reverse microemulsion coupled with the PDCs was investigated to allow single-step synthesis of nanocomposite membranes with mixed oxide and metallic phases *in situ* generated during the AHPCS-to-SiC conversion. This combination was already explored by Kaskel et al. to generate  $\text{CeO}_2$  nanoparticles inside SiC powders [49,50]. As mentioned before,  $\text{CeO}_2$  is an important oxidation catalyst for burning the carbon combustion residues from Diesel engine exhaust [16–19]. The combination of  $\text{CeO}_2$  with metal oxides such as  $\text{ZrO}_2$ ,  $\text{CuO}$ ,  $\text{Fe}_2\text{O}_3$  strongly improves the activity and stability of  $\text{CeO}_2$ -based catalysts according to the fact that they usually exhibit high surface reducibility. In particular Fe-doped  $\text{CeO}_2$  catalysts were demonstrated as very active for soot combustion due to the strong Ce–O–Fe interactions [20, 60–65]. If these nanocatalysts are dispersed in a SiC matrix, we expect to keep the filtration efficiency and durability of the membrane while minimizing or even preventing the sintering and agglomeration of the nanocatalysts during operating conditions and as a consequence improving the catalytic activity of SiC for HC/CO oxidation and soot combustion. Thus, we apply a reverse AHPCS-based microemulsion to generate new Ce–O–Fe–Pt (mixed oxide and metallic phases)/SiC membranes coated on DPF after dip-coating and pyrolysis under argon. These materials are tested with regard to CO/HC oxidation and soot combustion. The

membranes composed of mixed oxide and metallic phases dispersed in a SiC matrix demonstrate high catalytic performance for CO/HC oxidation and soot combustion.

From a scientific point of view, the paper is based on novelties at different levels: The SiC membrane and the characterization using soot loading experiments, the proposed combination of materials (mixed oxide and metallic phases dispersed in a SiC matrix) and the demonstration of the catalytic activity of the SiC membrane.

## 2. Experimental part

### 2.1. Materials

Two commercially-available preceramic polymers have been used. Allylhydridopolycarbosilane (AHPCS labeled SMP-10, Starfire Systems<sup>®</sup> Incorporation, New York, USA) with a density of  $0.998 \text{ g cm}^{-3}$  was used as-received and diluted in Tetrahydrofuran (Acros Organics, 99.85%, Extra Dry, AcroSeal<sup>®</sup>) to form various solutions with controlled AHPCS:THF ratios. SMP-10 is a clear, amber-colored, viscous liquid. SPR-036 is a commercial polycarbosiloxane containing both Si–C and Si–O bonds. It is a clear, low viscous transparent liquid with a density of  $1.1 \text{ g cm}^{-3}$  which represents a silicon oxycarbide (Si–C–O) ceramic precursor (Polyamic<sup>®</sup> SPR-036, Starfire Systems<sup>®</sup> Incorporation, New York, USA). It was used as-received and diluted in THF according to the ratio of AHPCS:THF that gives the membranes with the best performances. Cerium (III) nitrate hexahydrate ( $\text{Ce}(\text{NO}_3)_3 \cdot 6\text{H}_2\text{O}$ , Sigma-Aldrich, 99%), Iron nitrate ( $\text{Fe}(\text{NO}_3)_3 \cdot 9\text{H}_2\text{O}$ , Sigma-Aldrich,  $\geq 99.95\%$ ), Igepal<sup>®</sup> CA-520 (Average  $M_n \sim 427 \text{ g/mol}$ ; Sigma-Aldrich, 99%), n-Hexane (Acros Organics, 97%, Extra Dry over Molecular Sieve, AcroSeal<sup>®</sup>), ammonium hydroxide solution (Sigma Aldrich) were used without further purifications. Lab-scale DPF labeled as DPF without blocking inside the channels (2.5 cm of diameter and 7.6 cm of length with an average porosity of 43.1%) were provided by Ceramiques Techniques Industrielles (CTI corporation, Salindres, France). DPF are made of SiC grains consolidated with a silica binder and an inter-granular porosity of  $20 \mu\text{m}$  (Fig. 1). Before using them, lab-scale DPF were cut into smaller pieces (8 mm in width and height, 10 mm length) labeled

as miniDPF (Fig. 1) to optimize the membrane elaboration process. DPF samples were washed with water and acetone, dried at  $120 \text{ }^\circ\text{C}$  in an oven then heat-treated at  $600 \text{ }^\circ\text{C}$  (dwelling time of 2 h) under dynamic vacuum ( $5.10^{-1} \text{ mbars}$ ), then introduced in a glove-box for dip-coating.

### 2.2. Preparation of SiC and SiCO membranes

The dip-coating devices were placed in a glove-box under argon atmosphere. Different concentrations (10, 20, 30 and 40 vol%) of polymer in THF were prepared to tailor the polymer viscosity for dip-coating. The miniDPF and DPF samples were vertically dipped in the solutions kept under stirring to guarantee homogeneity of the mixture. The dip-coating device allows to control the dipping speed, ranging from  $0.1$  to  $14.5 \text{ cm}^{-1}$ . Once the support has been coated, it is deposited on an adsorbent paper during 1 h to allow evaporation of the solvent and remove the excess of coating solution at the surface of the honeycomb monoliths. Finally, coated monoliths were transferred into a silica tube inserted in a horizontal tube furnace (Nabertherm GmbH, Germany). The tube was pumped under vacuum and refilled with argon (99.995%). Subsequently, the samples were subjected to cycles of ramping of  $1 \text{ }^\circ\text{C min}^{-1}$  to  $1000 \text{ }^\circ\text{C}$  under argon, dwelling there for 2 h, and then cooling down to room temperature (RT) at  $2 \text{ }^\circ\text{C min}^{-1}$  to deliver the SiC and SiCO-coated DPF depending on the use of the polymer.

It should be mentioned that, for pressure loss tests, DPF samples were coated with the solution of SMP10 and SPR036 according to the optimized parameters (polymer concentration, dipping speed, immersion time) selected with miniDPF samples. Then, channels of the coated DPF were blocked after pyrolysis to test them for pressure loss tests.

### 2.3. Preparation of Ce–O–Fe–Pt/SiC membrane coatings

The nanocomposite Ce–O–Fe–Pt/SiC coatings were prepared according to a “water in oil” microemulsion or reverse micelle. 3 g of  $\text{Ce}(\text{NO}_3)_3 \cdot 6\text{H}_2\text{O}$  (6.91 mmol), 0.3 g of  $\text{Fe}(\text{NO}_3)_3 \cdot 9\text{H}_2\text{O}$  (0.74 mmol) and 0.1 g of  $\text{Pt}(\text{NH}_3)_4(\text{NO}_3)_2$  (0.258 mmol) were dissolved in water (8 mL), and then the oil phase n-hexane (90 mL) were added before addition of a definite quantity (10 mL) of Igepal

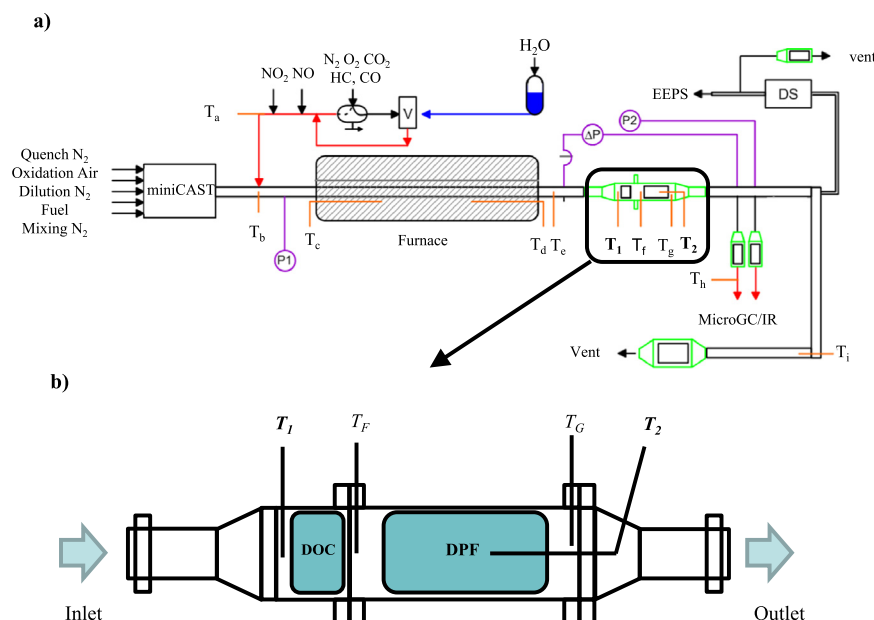


Fig. 1. Synthesis Gas Test Bench setup (a) and reactor to fix the mini-DPF and a mini-DOC (Diesel Oxidation Catalyst).

CA-520 as a surfactant to be mixed in a defined  $R_w$  ratio ( $R_w = n_{\text{water}}/n_{\text{surfactant}}$ , water number of mole divided by the surfactant molar number) of 16 at RT. This value allowed obtaining micelle particles with size ranging from 6 to 16 nm. The solution was maintained under vigorous stirring during 1 h at RT. Afterwards, the addition drop by drop of diluted ammonia solution led to the precipitation of the micelles. The mixture was kept for 1 h at RT under stirring. AHPCS (8.9 mL, 183.9 mmol based on the monomeric unit of AHPCS) was then added to the mixture and the solution was again stirred during 1 h at RT. The volatile compounds water and *n*-hexane, were partially removed under vacuum ( $55\text{ }^\circ\text{C}/1.5.10^{-1}$  mbar) using an ether bridge. An excess of acetone (150 mL) was poured in the solution to guarantee a well dispersion of the particles inside the matrix and the mixture was stirred during 24 h at RT before a second distillation under vacuum at ( $65\text{ }^\circ\text{C}/1.5.10^{-1}$  mbar) using an ether bridge to generate a liquid compound adapted to dip-coating. Solutions were then applied for dip-coating as described previously. A first pyrolysis step was achieved in a silica tube inserted in a horizontal tube furnace (Nabertherm GmbH, Germany). The tube was pumped under vacuum and refilled with argon (99.995%). Subsequently, samples were subjected to cycles of ramping of  $1\text{ }^\circ\text{C min}^{-1}$  to  $1000\text{ }^\circ\text{C}$ , dwelling there for 2 h, and then cooling down to RT at  $2\text{ }^\circ\text{C min}^{-1}$  to deliver the catalytic phase inside the SiC matrix. Then, a second pyrolysis step was performed in a muffle furnace under air at  $700\text{ }^\circ\text{C}$  during 2 h (heating rate  $5\text{ }^\circ\text{C min}^{-1}$ ) to remove residual carbon coming from the surfactant.

#### 2.4. Characterization

The rheological measurements of AHPCS were performed with the rotational MC 301 Paar-Physica rheometer, plate and plate geometry (50 mm diameter, 0.2 mm gap). The oscillatory tests were realized at constant strain amplitude,  $\gamma_a = 0.01$  [–], in controlled argon atmosphere ( $< 0.1\%$  oxygen and  $< 1\%$  moisture). The simple shear experiments, both strain and stress controlled, were done in air. The viscosity of the AHPCS homogeneous solutions were measured with a viscometer (Brookfield digital DV-1+) and with the solution under continuous stirring to keep the homogeneity. X-ray diffractograms were obtained with an X'Pert Pro diffractometer, using copper  $K_\alpha$  radiation ( $\lambda = 1.5406\text{ \AA}$ ). The pore volume, the percentage of porosity and the pore size distribution was obtained with mercury porosimetry measurements (AutoPore IV 9500, Micromeritics). SEM observation has been made using an Hitachi S4800 microscope, and EDX measurement with an Hitachi S4500 coupled with a Thermofischer Scientific Nanotracer Si(Li) detector. To obtain a cross-sectional view, samples have been cut and put into a resin before observation.

#### 2.5. Tests for pressure loss

Measurements are made on an ambient air flux bench. Three different flows are tested ( $35,000$ ,  $120,000$  and  $200,000\text{ h}^{-1}$ ). We used such values because they are included in the space velocity range in a Diesel exhaust:  $35,000\text{ h}^{-1}$ : lowest range and  $200,000\text{ h}^{-1}$ : highest range).

The pressure loss is obtained in mbar and corresponds to the difference of pressure between the inlet and outlet of the filter (i.e. at a length of 5 times of the diameter before and 10 times of the diameter after the monolith).

#### 2.6. CO and HC oxidation, soot combustion and filtration efficiency tests on Synthetic Gas Bench (SGB)

Tests were performed in a Diesel-like feed gas (described in Table 1) by fitting samples in a reactor set-up in a controlled oven.

**Table 1**

Laboratory feed gas composition.

CO/H <sub>2</sub>	HC	NO	CO <sub>2</sub>	O <sub>2</sub>	H <sub>2</sub> O
500/167 ppm	150 ppmC1 (75% C <sub>3</sub> H <sub>6</sub> +25% C <sub>3</sub> H <sub>8</sub> )	150 ppm	5%	13%	10%

The tests allow simulating transitory system with pulsated injections. Dihydrogen (H<sub>2</sub>) is added to the feed gas to respect a 3/1 ratio between CO and H<sub>2</sub>.

The gas generation was handled automatically with a computer and the gas composition as well as the gas flow (CO/H<sub>2</sub>: 500/167 ppm; HC: 150 ppm (75% C<sub>3</sub>H<sub>6</sub>+25% C<sub>3</sub>H<sub>8</sub>); NO: 150 ppm; CO<sub>2</sub>: 5%; O<sub>2</sub>: 13%; H<sub>2</sub>O: 10%) diluted in nitrogen were controlled independently with a mass flow controller allowing to eliminate all external perturbations like the temperature or the pressure variations. HC on NOx ratio is defined as the ratio between HC (in ppmC1) and NOx (ppm) upstream of the catalyst. The reductants are delivered by a precision volumetric pump and vaporized in an in-house system. One gas hourly space velocity (SV) has been tested:  $40,000\text{ h}^{-1}$ . The steam was added to the gas mixture by a humidifier and a temperature programmed infrared furnace allowing heating the all gas mixture. The sample was heated by the gas mixture flowing (with a heating rate of  $1\text{ }^\circ\text{C min}^{-1}$ ) into the channels. The Synthesis Gas Test Bench (SGB, Fig. 1) combined five gas analyzers connected to a computer allowing to measure simultaneously total hydrocarbon (THC), CO, CO<sub>2</sub>, O<sub>2</sub>, NO, NO<sub>2</sub> and N<sub>2</sub>O.

The determination of the catalytic activity was done by a comparative analysis of the gas composition between the upstream and downstream section of the sample, and also regarding the temperature. After the stabilization of the temperature and the gas composition, light-off measures were made with a temperature ramp of  $1\text{ }^\circ\text{C min}^{-1}$  from  $80$  to  $400\text{ }^\circ\text{C}$ . Three cycles of light-off were made for each sample.

Tests for soot combustion and filtration efficiency were made at IRCELYON (France) by using a SGB described elsewhere [66], Fig. 1a. Soot particles were produced by a mini Combustion Aerosol Standard burner (miniCAST, Jing Ltd. Switzerland). In addition, O<sub>2</sub>, C<sub>3</sub>H<sub>8</sub>, C<sub>3</sub>H<sub>6</sub>, CO, NO and N<sub>2</sub> were introduced to complete the miniCAST mixture and make a total flow of  $1200\text{ NL/h}$ . A stainless steel reactor was used to fix the mini-DPF ( $1 \times 3\text{ in.}$ ) as well as a mini-DOC (Diesel Oxidation Catalyst,  $1 \times 1\text{ in.}$ ) placed upstream the mini-DPF (Fig. 1b). The reactor was placed downstream of the tubular oven, inside an isolated chamber. The temperature control was performed by a retrofitted closed loop control system which controls the temperature at the exit of the oven (inlet of the reactor) and allows reaching up to  $700\text{ }^\circ\text{C}$ . Before being placed in the reactor, mini-DPFs were wrapped in a vermiculite-coated fiber mat which provided insulation and prevented gas and PM by-pass. Once the samples were introduced in the reactor, they were calcined at  $700\text{ }^\circ\text{C}$  for 4 h in order to allow thermal expansion of the fiber mat and keep it firmly in place during operation. The reactor is equipped with four chromel-alumel thermocouples (type K) in order to obtain a detailed temperature profile of the studied samples. The pressure drop produced by mini-DPFs was measured by different pressure sensors (Keller) located at the inlet and the outlet of the reactor. A micro gas chromatograph ( $\mu\text{GC}$ , R 3000 SRA) was used for the analysis of C<sub>3</sub>H<sub>8</sub>, C<sub>3</sub>H<sub>6</sub>, and O<sub>2</sub>; a chemiluminescence detector (ECO Physics CLD 62) for the detection of NO, NO<sub>2</sub> and NOx; and an on-line Infrared analyzer (EMERSON, NGA 2000) for the analysis of CO, CO<sub>2</sub>, N<sub>2</sub>O and H<sub>2</sub>O. The particulate number (PN) and the size distribution were measured by an engine exhaust particle sizer spectrometer (EEPS model 3090, TSI Inc.) An injection diluter (Palas VKL 100, dilution ratio 1:230) was used in order to obtain

PN below the upper measurement range of the EEPS. The first part of these tests was consisted of a soot loading step of the sample for 1 hour with a rate of 28 mg of soot per hour (particle size around 93.1 nm with dispersion between 40 and 200 nm) at 200 °C (temperature of the DOC). The feed was composed of 8.6% CO<sub>2</sub>, 0.5% CO, 0.1% C<sub>3</sub>H<sub>6</sub>, 0.1 C<sub>3</sub>H<sub>8</sub>, 500 ppm NO, 2.6% H<sub>2</sub>O, 10% O<sub>2</sub> in nitrogen. Then, the flame of the CAST burned was stopped and after 20 min of stabilization, a Temperature Programmed Oxidation (TPO) experiment was performed from 200 °C up to 555 °C (temperature of the DOC) with a heating ramp of 10 °C min<sup>-1</sup>. The pressure drop and the gas concentrations have been monitored as a function of the temperature.

### 3. Results and discussion

The choice of the organosilicon polymers is a key consideration to obtain the targeted materials. There are two types of commercially-available organosilicon polymers to prepare SiC. They display the structural configuration [-Si-C-]<sub>n</sub>. Yajima et al. reported in 1975 the preparation of β-SiC through pyrolysis of methyl-substituted polysilanes, namely polycarbosilanes (PCS) [67–69]. PCS, a solid, fusible and soluble preceramic polymer, has been investigated as a precursor for SiC fibers for over 30 years. However, the preparation of supported membranes is procedurally difficult because of solid state and the low ceramic yield of PCS and the dimensional changes which occur during the pyrolytic conversion into SiC. An idealized SiC coating precursor for this kind of application would meet the following requirements: an adequate ratio of Si to C, viscoelastic properties (e.g. solubility) to facilitate procedural handling and a sufficiently high molar

mass to avoid oligomeric volatilization to grant a higher ceramic yield. To address the requirement for solubility and high ceramic yield, complex polycarbosilane structures (network or branched) have to be taken into account. Hyperbranched Allylhydridopolycarbosilane (AHPCS), a co-polymer, was designed to produce near-stoichiometric SiC [58,59]. Compared with PCS, AHPCS is much more processable. It is liquid and it displays a higher ceramic yield which results in a lower volume shrinkage during the polymer-to-ceramic conversion. Furthermore, it can be chemically modify to integrate catalytic active phases. Within this context, AHPCS appeared to us as the best candidate for producing the SiC-based membranes supported on DPF. The sequence which illustrates the design of these materials is depicted in Fig. 2.

#### 3.1. Rheological properties of AHPCS

Rheology is a key aspect that affects the shaping of preceramic polymers and therefore the properties of shaped ceramics [70–72]. As a representative preceramic polymer for dip-coating, AHPCS needs to fulfill particular requirements which are mainly based on its chemistry: it has to be liquid, soluble, characterized by a small viscosity and almost lack of elasticity. AHPCS is a pure viscous liquid (without elasticity) with a Newtonian behavior (relatively stable viscosity according rheological measurements) and displays a viscosity in the range of 40 mPas to 100 mPas depending on the temperature (Fig. 3).

Fig. 3 The viscosity decreases from 97 mPas (20 °C) to 41 mPas (50 °C) and no enhanced cross-linking and decomposition occur by increasing the temperature of exposure of AHPCS. However, such values of viscosity are too high to appropriately coat the

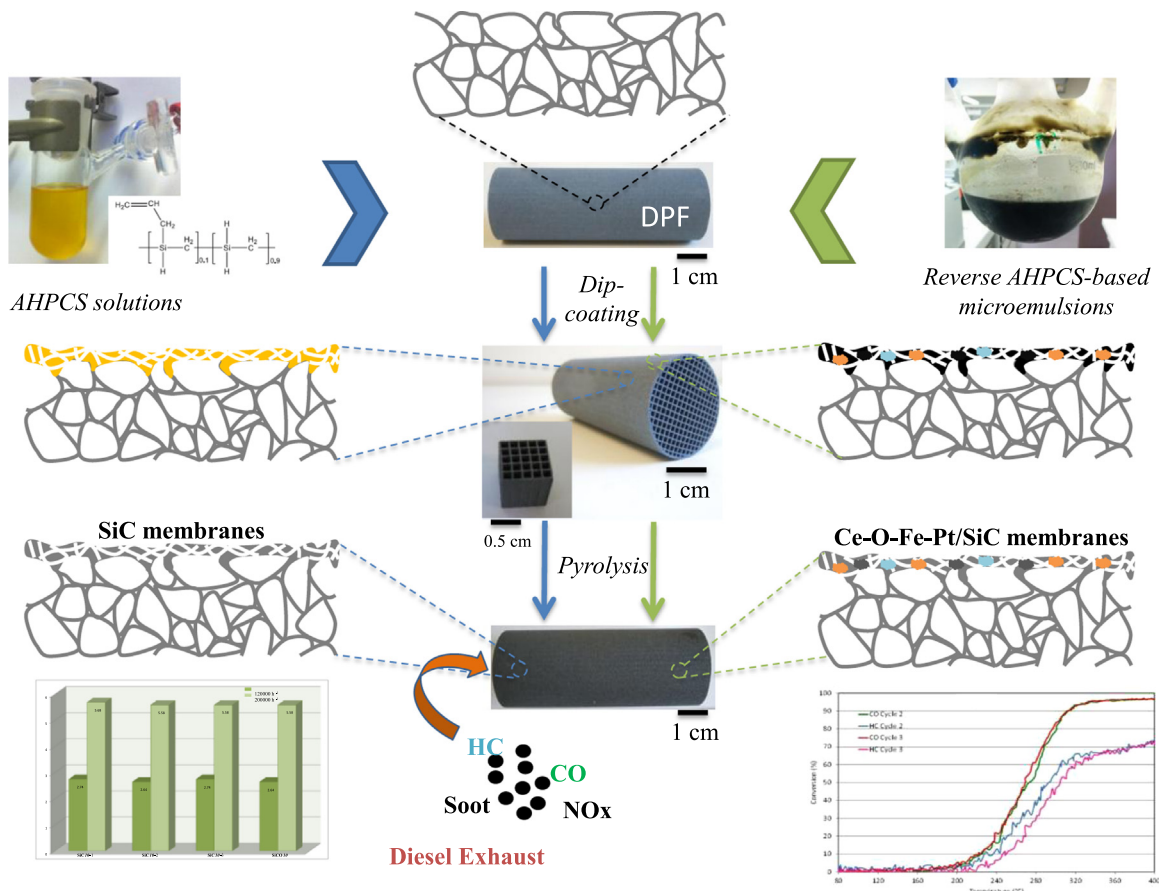
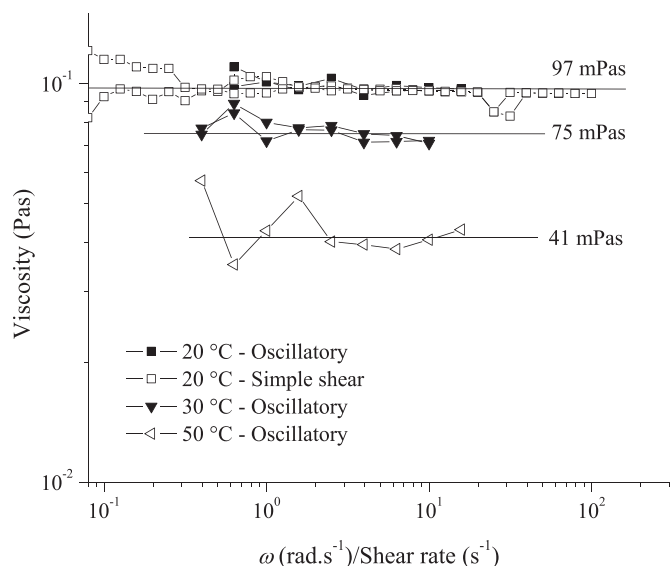


Fig. 2. Sequence illustrating the design of AHPCS-derived SiC and Ce-O-Fe-Pt/SiC membranes.



**Fig. 3.** Viscosity function of AHPCS as function of temperature and frequency, respectively shear rate. Experiments performed at 50 °C are in the limit of the torque transducer sensitivity.

**Table 2**  
Viscosity of the four diluted AHPCS solution measured at RT.

Vol% AHPCS in THF	10	20	30	40
Samples	<b>AHPCS10</b>	<b>AHPCS20</b>	<b>AHPCS30</b>	<b>AHPCS40</b>
Viscosity (mPas)	4.5–4.8	4.9–5.0	5.9–6.0	8.1–8.2

internal porosity of DPF. Within this context and according to the good solubility of AHPCS in THF, we suggested modifying the rheological properties of AHPCS by dilution in THF. We have

prepared a set of four AHPCS solutions diluted in THF (10 (**AHPCS10**), 20 (**AHPCS20**), 30 (**AHPCS30**) and 40 (**AHPCS40**) vol% of polymer in THF). These solutions have been prepared to evaluate the effect of the viscosity; therefore the concentration of polymer in THF (Table 2), on the modification of DPF after pyrolysis along with the influence of the dip-coating parameters. As expected, the viscosity significantly decreased in line with the decrease of the concentration of AHPCS in THF. The viscosity is seen to be quite similar between the different solutions. These solutions have been used to coat the channels of DPF by dip-coating. Dip-coating was achieved in a glove-box according to the sensitivity of AHPCS with air and moisture. This is clearly confirmed by following the time evolution of the viscosity of **AHPCS30** in air (See Fig. 1SI in Supporting Information). In this experiment, the measured sample viscosity is increasing from 5.85 mPas to 8.8 mPas. Therefore, particular attention is required to coat miniDPF and DPF without contact with air and moisture to obtain the expected ceramic composition. Once dip-coating has been achieved, the AHPCS-coated miniDPF (or DPF) is introduced in a furnace without air contact and then subjected to a cycle of pyrolysis at 1 °C min<sup>-1</sup> up to 1000 °C (dwelling time of 2 h). It should be mentioned that the pyrolysis temperature was deliberately programmed at 1000 °C to generate a sufficiently stable SiC and prevent crystallization that could involve the appearance of cracks through the coating. During the pyrolysis, the polymer is subjected to a weight loss (~28%, (See Fig. 2SI in Supporting Information)), transformed into amorphous SiC (See Fig. 2SI as inset in Supporting Information) and generates SiC membrane-coated miniDPF. The samples were labeled according to their initial concentration of AHPCS in THF from **SiC10** (from **AHPCS10**) to **SiC40** (from **AHPCS40**). Membrane-coated DPFs were systematically analyzed by SEM after dip-coating and pyrolysis.

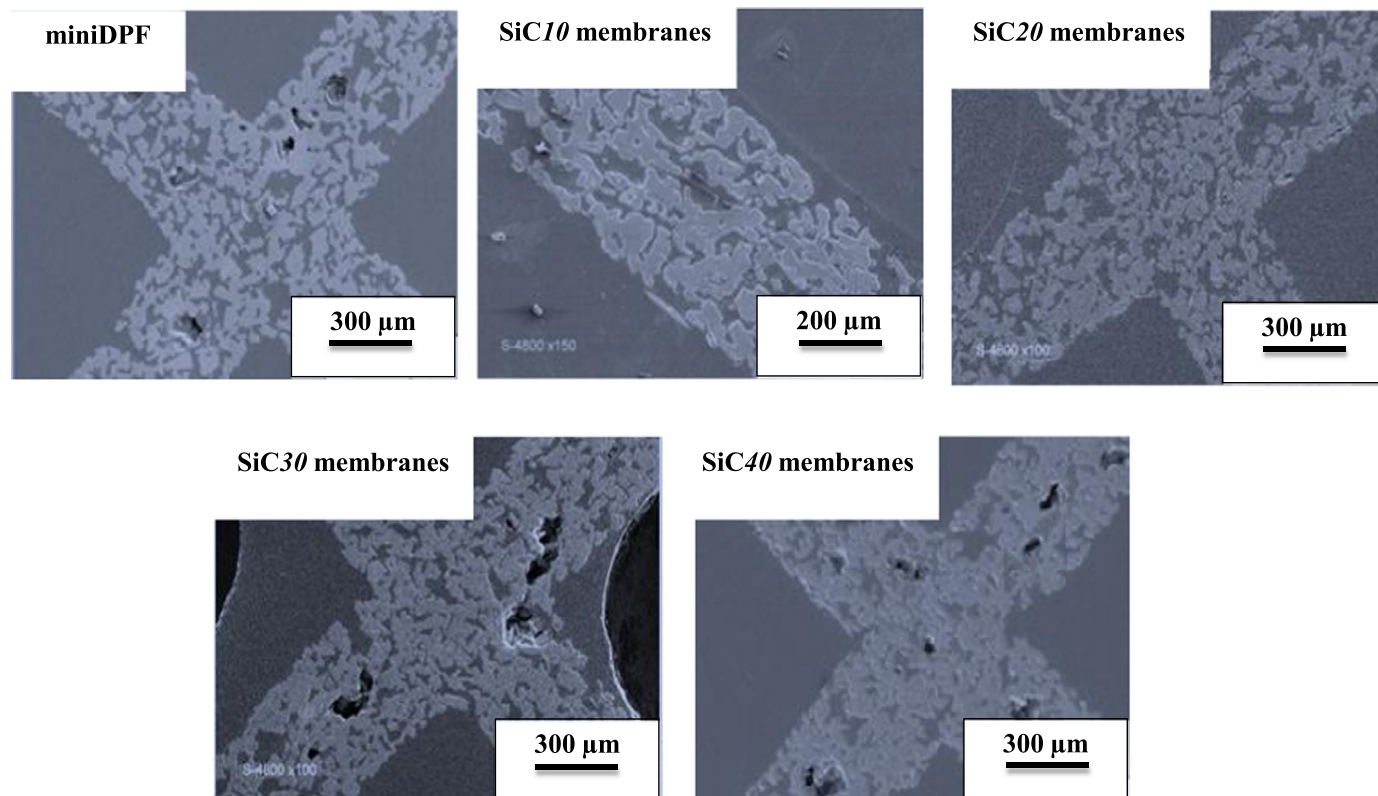


**Fig. 4.** SEM pictures of the cross-section of miniDPF and miniDPF coated with **SiC10**→**40** membranes integrated in a resin.

### 3.2. Preparation of SiC membrane-coated miniDPF

It should be mentioned that the dipping speed (of dip-coating) as well as the immersion time have no negative effect on the porosity of DPF using the same formulation. As a consequence, a high dipping speed ( $=14.5 \text{ cm min}^{-1}$ ) associated with a short immersion time ( $=1 \text{ min}$ ) have been fixed. Within this context, the concentration of AHPCS is demonstrated to be the key factor that affects the porosity of DPF as shown in Fig. 4. Fig. 4 reports the SEM images of the SiC membrane-coated miniDPF samples integrated into a resin to observe the cross-section of samples.

The initial structure of the miniDPF support shows a relatively good distribution of the open and interconnected porosity. Other SEM images are available in Fig. 3SI (See Supporting Information). After coating, a decrease of the porosity is observed in line with the increase of the AHPCS concentration in the coating solution. The initial porosity is gradually filled with the increase of the AHPCS content of the solution. This is clear by comparing the SiC10 and SiC40 membrane-coated miniDPF. In the SiC40 membrane-coated miniDPF, the porosity is considerably reduced which is expected to affect the filtration efficiency.

To better qualify and quantify the macroporosity of the different samples, mercury intrusion porosimetry investigations have been performed. Cumulative intrusion curves of initial support and coated DPF have been compared (Fig. 5).

Here, we have to specify that mercury porosimetry provides information only on the features that control the mercury intrusion—the windows that connect adjacent macropores—and not on the macropore diameters themselves. The first important feature is that the membranes are robust enough to endure mercury impregnation without collapsing. Secondly, there are two types of behavior: the virgin miniDPF and the membrane-modified miniDPFs.

The curve of cumulative pore volume versus pore diameter showed a continuous increase in mercury uptake with a decrease in pore diameter (i.e., increase of Hg intrusion pressure) for all samples. The pore volume and size distribution of the virgin miniDPF revealed one intrusion step above  $10.5 \mu\text{m}$ . The total pore volume measured by this method is  $0.263 \text{ cm}^3 \text{ g}^{-1}$ , whereas the cell junction diameter is measured to be  $21.83 \mu\text{m}$ . From the cumulative pore volume, the porosity of the sample is calculated to be 43.1%. It should be mentioned that bulk and apparent densities of  $1.64$  and  $2.88 \text{ g cm}^{-3}$  are found, respectively.

A decrease of the mercury cumulative intrusion was observed along with the increase of the concentration of AHPCS in the solution from samples SiC10 to SiC40. Two intrusion steps are identified in the domain of macropores with, for example, one above  $10.5 \mu\text{m}$  and a second one from  $3$  to  $10.5 \mu\text{m}$  for the sample SiC10 indicating a broadening of the distribution of the pore diameters in these samples (Fig. 5 as inset). It is clear that the

**Table 3**  
Mercury-intrusion porosimetry of miniDPF, SiC10→40 membranes and SiC010 membrane.

	miniDPF	SiC10	SiC20	SiC30	SiC40	SiC010
Total intrusion volume (mL/g)	0.263	0.235	0.225	0.207	0.205	0.24
Average pore size diameter (Volume) ( $\mu\text{m}$ )	21.8	18.6	18.2	18.3	18.7	17.7
Porosity (%)	43.1	40.1	37	35.9	35.3	40.9

monoliths display a cell window with a relatively large polydispersity in size which corresponds to the size of the larger interstices between the primary macroporous particles and an additional macroporosity created by the membrane coating. By applying a coating membrane from only 10 vol% of polymer (sample SiC10), all characteristics of the initial DPF are lowered as it is showed in Table 3.

The total pore volume measured by this method is  $0.237 \text{ cm}^3 \text{ g}^{-1}$ . The cell junction diameter decreased to  $18.3 \mu\text{m}$  while the SiC10 membrane-coated miniDPF retained a relatively high apparent porosity ( $=40.1\%$ ) from the cumulative pore volume which is expected to allow trapping larger number of finer particles. It should be mentioned that bulk and apparent densities of  $1.64$  and  $2.67 \text{ g cm}^{-3}$  are found, respectively. By increasing the concentration of AHPCS in the solvent, the curve of cumulative pore volume versus pore diameter shows the same trend: a continuous increase in mercury uptake with a decrease in pore diameter (i.e., increase of Hg intrusion pressure). As a direct consequence of the increase of the concentration of the polymer in the solvent, both the mercury intrusion volume and the macroscopic porosity gradually decrease from SiC10 to SiC40: From the cumulative pore volume, the porosity of the sample SiC20, SiC30 and SiC40 is calculated to be 37%, 35.9% and 35.4%, respectively. Also, the material bulk density increases from  $1.64 \text{ g cm}^{-3}$  (SiC20) to  $1.72 \text{ g cm}^{-3}$  (SiC40) as the polymer content is increased in the solvent, because the shell thickness increases. Finally, the skeletal density and the cell junction diameter remain approximately unaffected at around  $2.65 \text{ g cm}^{-3}$ , and  $18.5 \pm 0.2 \mu\text{m}$ , respectively.

By coupling SEM and mercury porosimetry results, it appears that the miniDPF coated with the SiC10 membrane represents the best compromise for us because it sufficiently reduces the cell junction diameter without affect to much the level of porosity which is required to combine filtration efficiency and limited pressure drop. Furthermore, because of the small required amount of AHPCS, this limits the cost of the material for industrial applications.

Interestingly, changing the nature of the polymer (from SMP-10 to SPR-036) and keeping the same polymer concentration in THF

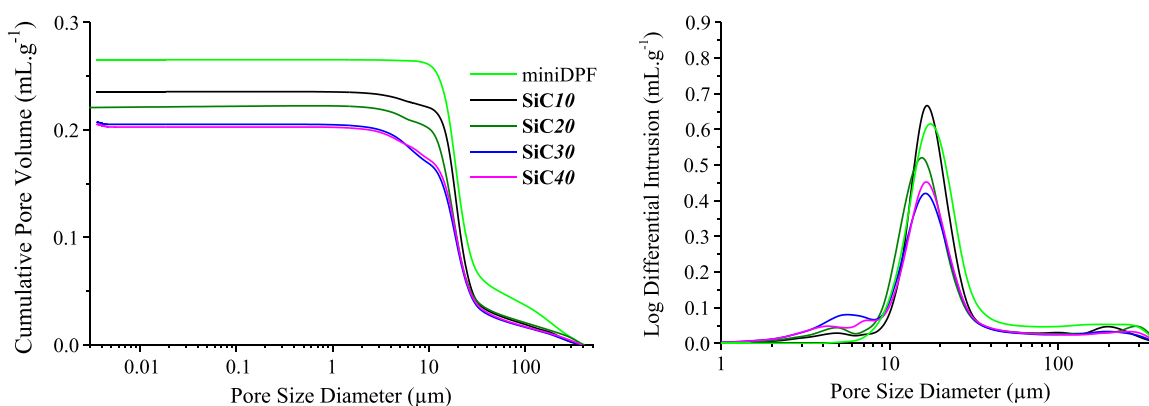


**Fig. 5.** Macroscopic pore-size distribution obtained by mercury-intrusion porosimetry of miniDPF and miniDPF coated with SiC10→40 membranes.

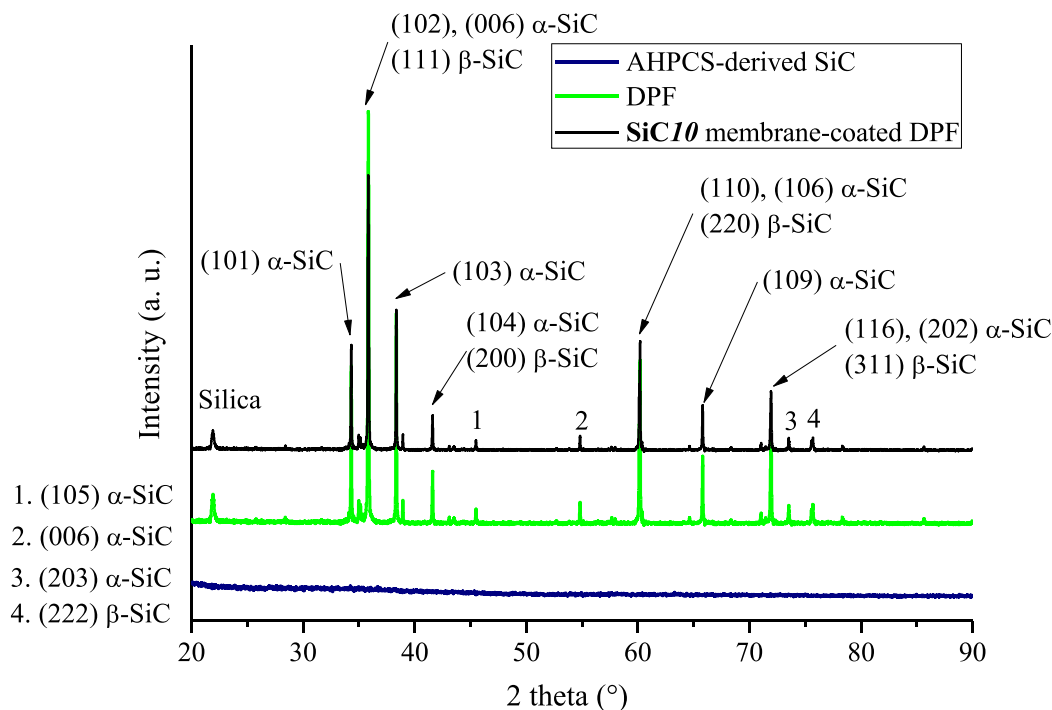


Fig. 6. XRD pattern of AHPCS-derived SiC, DPF and the SiC10 membrane-coated DPF.

(10 vol%), dip-coating and pyrolysis parameters, we were able to obtain **SiC10** membrane-coated miniDPF with similar textural properties (Table 3). This clearly proves the versatility of our approach. In the following section, the **SiC10** membrane-coated DPF is characterized by XRD, EDX, high temperature TGA, SEM and pressure loss tests.

### 3.3. Characterization of the SiC10 membrane-coated DPF

AHPCS-derived SiC are X-ray amorphous after pyrolysis at 1000 °C, according to the broadening of the background peaks as shown on the XRD pattern (Fig. 6). In contrast, the  $\beta$ - and  $\alpha$ -SiC are identified as the major phases in DPF. Cubic  $\beta$ -SiC is identified by the presence of highly intense peaks at 35.65° ( $d=2.516$  Å), 41.40° ( $d=2.179$  Å), 60° ( $d=1.540$  Å), and 71.78° ( $d=1.314$  Å). The presence of hexagonal polytypes of SiC (6 H, 2 H, and 4 H) is identified by the presence of two additional highly intense peaks at 34.08° ( $d=2.628$  Å), 38.15° ( $d=2.357$  Å) and 61.4° ( $d=1.508$  Å).

The XRD pattern is composed of the other peaks characteristic of the  $\beta$ -SiC and  $\alpha$ -SiC phases as well as of the silica (peak at around 21.8°)

Fig. 6 As expected, the XRD peaks of the **SiC10** membrane-coated DPF does not change in comparison to DPF according to the low thickness of the membrane. The SEM image of a fragment of the sample coated with the **SiC10** membrane (Fig. 7) indicates that DPF is homogeneous covered with a porous layer on top.

Fig. 7 The membrane thickness is estimated as low as ~150 nm. Energy Dispersive X-ray Spectroscopy (EDXS) analysis reveals a typical chemical formula of  $\text{Si}_{1.0}\text{C}_{1.2}\text{O}_{0.2}$  (Fig. 4SI, See Supporting Information). According to the chemical formula found for DPF ( $\text{Si}_{1.0}\text{C}_{0.6}\text{O}_{1.1}$ ), the relatively low O content is attributed to the presence of the SiC membrane. Furthermore, free carbon is also present in the form of graphite-like nano-domains, graphene-like sheets or turbostratic carbon in the membrane as commonly observed for polymer-derived SiC.

The high-temperature behavior of DPF and **SiC10** membrane-coated DPF has been investigated by HT-TGA up to 1500 °C under argon (Fig. 8).

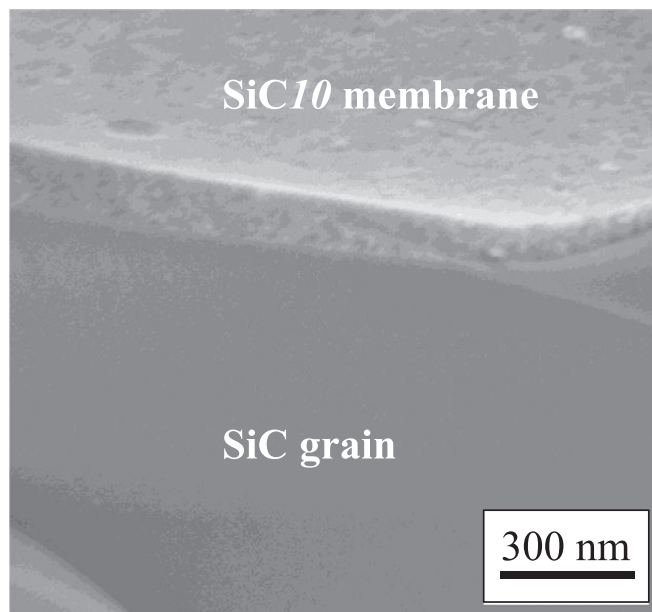
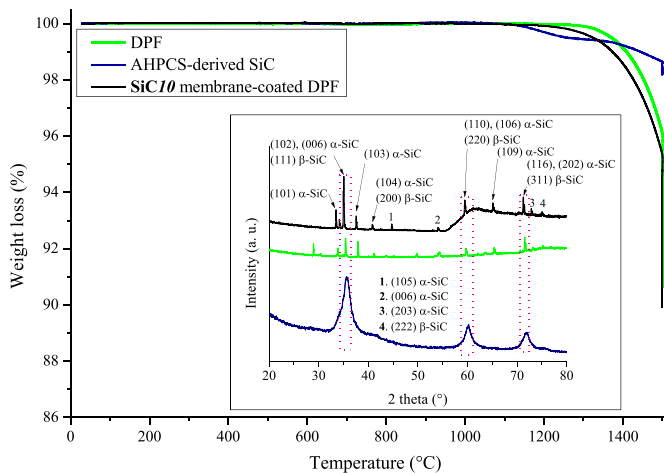


Fig. 7. SEM image of the miniDPF coated with the **SiC10** membrane.

The same treatment has been made on the AHPCS-derived SiC powders produced at 1000 °C under argon. The DPF and the **SiC10** membrane-coated DPF display the same TG profile with a weight loss that started at ~50 °C lower for the **SiC10** membrane-coated DPF in comparison to the virgin DPF. The final weight losses for these two samples are similar and relatively high (around 11% of weight loss) compared with AHPCS-derived SiC powders. Indeed, AHPCS-derived SiC powders show no mass change up to 1100 °C in flowing argon, demonstrating good stability of the amorphous SiC network. Above 1100 °C, the weight slowly changes most probably because of residual hydrogen evolution whereas heat-treatment at temperatures higher than 1350 °C results in another decomposition step associated with a continuous weight loss up to 1500 °C.



**Fig. 8.** High temperature TGA of AHPCS-derived SiC, DPF and the **SiC10** membrane-coated DPF under argon at 1500 °C. XRD patterns of DPF and the **SiC10** membrane-coated DPF heat-treated at 1500 °C appear as inset.

The total weight loss at 1500 °C is below 2%. XRD of the HT-TGA residues showed the disappearance of peaks attributed to silica as well as from DPF and from **SiC10** membrane-coated DPF which indicated the high silica content in DPF. As a consequence, Eq. (1) may be suggested as representative of the mechanism occurring during heat-treatment under argon up to 1500 °C.



XRD investigation also shows a general increase in crystallization degree of the AHPCS-derived SiC powders with increasing pyrolysis temperature. It shows the distinct diffraction peaks

which can be assigned to the (111), (220) and (311) reflections of cubic  $\beta$ -SiC after the increase of the annealing temperature to 1500 °C.

The microstructure of the heat-treated DPF and **SiC10** membrane-coated DPF has been characterized by SEM (Fig. 9).

The comparison of SEM images of fragments of the heat-treated DPF and **SiC10** membrane-coated DPF demonstrates the interest of the membrane to protect the DPF against crack formation. Cracks appeared in DPF after TG experiments performed at 1500 °C as shown in Fig. 9(b). In contrast, the coated DPF does not show surface modification. This result proposes that the **SiC10** membrane acts as a thermal barrier coating and allows producing a material with a better thermal stability, and therefore a better durability. It is suggested that Si–O moieties removed from DPF (Eq. (1)) reacts at high temperature with the free carbon [73] present in the AHPCS-derived SiC membrane to form Si(O)C leading to the formation of a better surface without cracks. It should be mentioned that polymer-derived amorphous ternary compounds of silicon (Si), oxygen (O) and carbon (C), i.e., Si(O)C, are thermodynamically metastable [74] and thus such a reaction can be viewed as effective in the current system.

Our approach for increasing the filtration efficiency is to use an additional fine porous filtration membrane on the filter wall as shown previously. However, this method is expected to affect the back pressure of the filter. In an attempt to further optimize the pressure drop and the filtration characteristics, the difference between the static pressure at entry and exit of the DPF is a fundamental performance criterion. The measurement is closely related to gas flow, gas composition, gas pressure and gas temperature (which is affected by DPF internal temperature). Experimental studies are carried out on the **SiC10** membrane-coated DPF to identify the role of the membrane on the properties of the

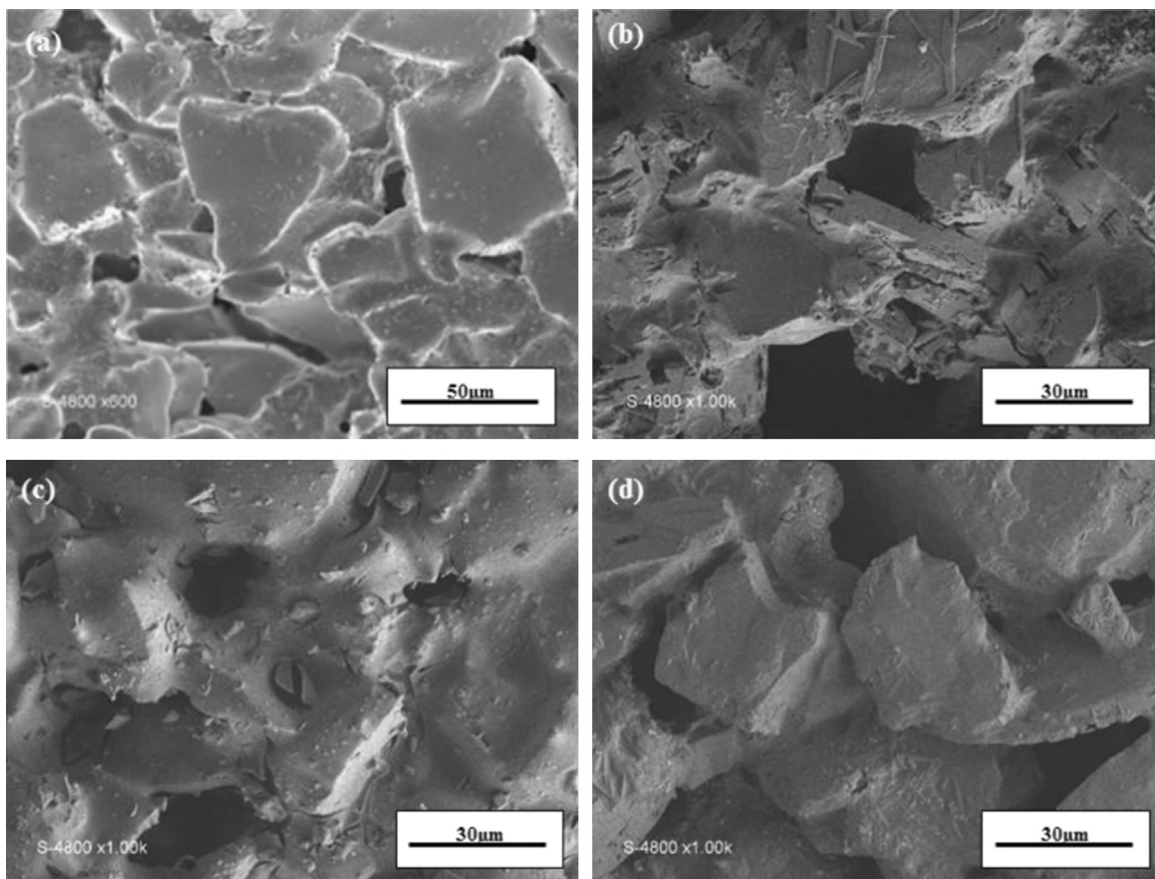


**Fig. 9.** SEM pictures of DPF before (a) and after HT-TGA (b) and **SiC10** membrane-coated DPF before (c) and after HT-TGA (d).

particulate filters. Pressure drop and filtration efficiency of the specimens have been investigated by means of reproducible soot loading experiments on a special laboratory test bench (Fig. 5SI, See Supporting Information). It consists in estimating the resistance of the samples against the air going through them. During application, the filter is filled with soot leading to a raise of the pressure loss. Each filter has a maximum pressure loss which corresponds to its limit for application. The data obtained from the charge loss tests using two different flows ( $12,000 \text{ h}^{-1}$  and  $200,000 \text{ h}^{-1}$ ) are reported in Fig. 10.

The virgin DPF displayed values between 5.3 and 5.7 mbars (pressure measured inlet and outlet the filter) for  $200,000 \text{ h}^{-1}$ . The tests for **SiC10** membrane-coated DPF were performed three times to demonstrate data reproducibility of the results. The tests show values within this pressure range of DPF which highlight that the membranes has no negative impacts on the filtration efficiency of DPF despite the fact that the cell junction diameter significantly decreased. Similar results have been obtained with the **SiCO10** membrane-coated DPF. As a consequence, an optimal balance between filtration efficiency and back pressure is obtained for the DPF whose top pore layers have been coated with the additional thin **SiC10** membrane. The filtration efficiency stays at approximately 99% during the overall filtration process which is equivalent to the virgin DPF. Furthermore, such a test has proved the good stability and adherence of the membrane on the DPF.

#### 3.4. Development of the catalytic activity of SiC-based coating membranes

Particle formation in reverse micelles is achieved through a multi-microemulsion route which takes advantage of three separately microemulsions prepared from  $\text{Ce}(\text{NO}_3)_3 \cdot 6\text{H}_2\text{O}$ ,  $\text{Fe}(\text{NO}_3)_3 \cdot 9\text{H}_2\text{O}$  and  $\text{Pt}(\text{NH}_3)_4(\text{NO}_3)_2$  of the same water/surfactant (Igepal CA-520)/oil (*n*-hexane) ratio. The principle for the design of Ce–O–Fe–Pt/SiC membranes supported on DPF is described in Fig. 11.

It should be mentioned that THF is added at the end of the AHPCS-reverse microemulsion for dip-coating. Pyrolysis is achieved under argon at  $1000 \text{ }^\circ\text{C}$  and is associated with a ceramic yield of 57% to convert the AHPCS-based micromemulsion into the Ce–O–Fe–Pt/SiC composites (Fig. 2SI, See Supporting Information) whereas the further heat-treatment in air at  $700 \text{ }^\circ\text{C}$  consists to remove residual carbon. XRD characterization shows that the

resulting material contains extremely diffuse XRD peaks (Fig. 2SI, See Supporting Information as inset) which could be attributed to fine crystallite size of the cubic phase of  $\text{CeO}_2$  ((111) peak ( $2\theta=29^\circ$ )) and  $\gamma\text{-Fe}_2\text{O}_3$  ((311) peak at  $35.5^\circ$ ). Beside this, diffuse peak characteristics of  $\beta\text{-SiC}$  ((220) peak ( $2\theta=60.1^\circ$ ) and (311) peak ( $2\theta=72.25^\circ$ )) can be identified whereas AHPCS-derived SiC was fully X-ray amorphous (Fig. 2SI, See Supporting Information as inset). This shows that the presence of the catalytic phases tends to slightly increase the crystallization rate of SiC. EDXS analyses confirmed the presence of the catalytically active phases (Fig. 6SI, See Supporting Information). As-obtained membranes are then analyzed on synthetic gas bench to evaluate their HC/CO oxidation as well as the soot combustion along with their filtration efficiency after the deposition of stopper in the coated channels.

##### 3.4.1. HC and CO oxidation tests

To evaluate the potential applicability in the catalytic activity for CO and HC oxidation, the catalytic performances of the Ce–O–Fe–Pt/SiC membranes supported on DPF in CO and HC oxidation have been evaluated under a reaction stream with a gas composition of  $\text{CO}/\text{H}_2$ : 500/167 ppm; HC: 150 ppm (75%  $\text{C}_3\text{H}_6$  + 25%  $\text{C}_3\text{H}_8$ ); NO: 150 ppm;  $\text{CO}_2$ : 5%;  $\text{O}_2$ : 13%;  $\text{H}_2\text{O}$ : 10% diluted in nitrogen. The blank experiment of soot combustion without catalyst, i.e., **SiC10** membrane-coated DPF, was also performed.

HC are oxidized to form carbon dioxide and water vapor whereas carbon monoxide is oxidized into carbon dioxide. The results are shown in Fig. 12 where the CO (a) and HC (b) conversion are reported as a function of the temperature.

First of all, it can be observed that the SiC material is not catalytically active. In contrast, the Ce–O–Fe–Pt/SiC membrane-coated DPF are active in the CO and HC oxidation tests. They showed an effective activity toward CO and HC reaching their maximum of activity at respectively  $335 \text{ }^\circ\text{C}$  and  $400 \text{ }^\circ\text{C}$ . The light-off temperature (temperature of 50% conversion,  $T_{50}$ ) is  $270$  and  $307 \text{ }^\circ\text{C}$ , respectively. The stability and activity was examined under the same conditions after successive cycles. Cycles 2 and 3 are compared in Fig. 11(c). The Ce–O–Fe–Pt/SiC membranes-coated DPF shows an activity for CO conversion reaching  $T_{50}=270 \text{ }^\circ\text{C}$  for both cycles which means that the material is stable under the imposed conditions.  $T_{50}$  reaches  $295 \text{ }^\circ\text{C}$  (Cycle 2) and  $310 \text{ }^\circ\text{C}$  (Cycle 3) for HC oxidation which indicates a deactivation of 5%. Iron seems to help for both gas removal but after the second cycle, his activity for HC does not manage to stabilize.

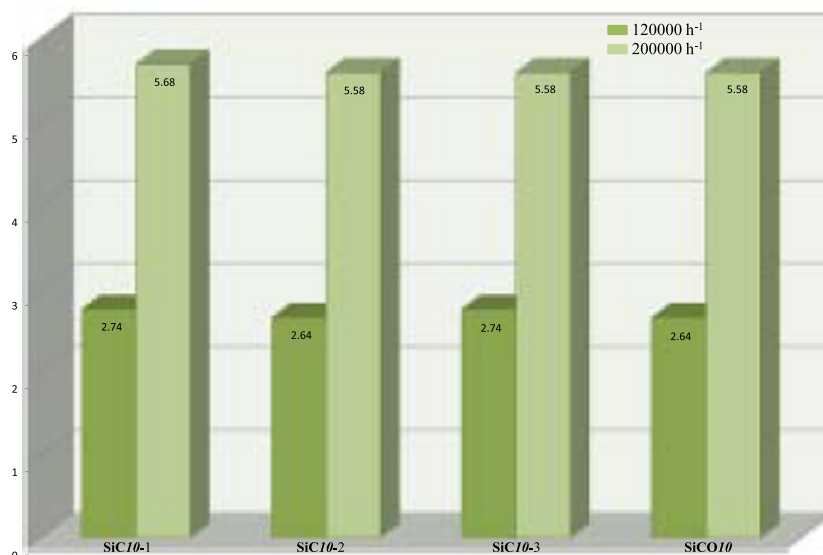
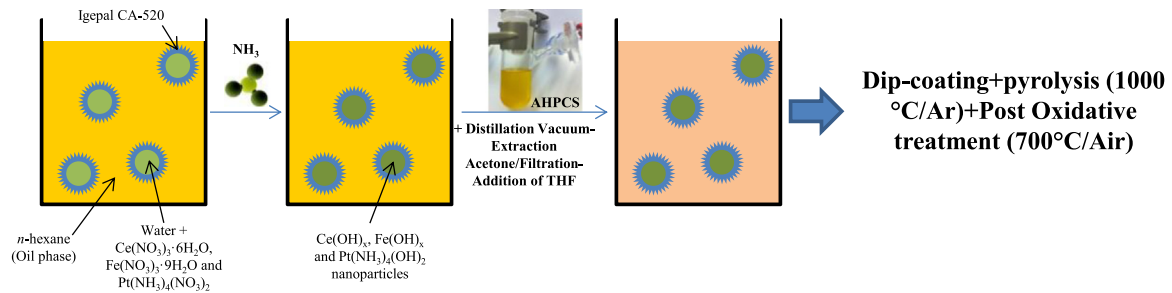


Fig. 10. Pressure loss tests for **SiC10** and **SiCO10** membrane-coated DPF.



**Fig. 11.** Schematic synthesis strategy to prepare Ce-O-Fe-Pt/SiC nanocomposite membranes supported on DPF.

There is a lack of evidence or discussion in the literature to support our observation with regards to the performance of the Ce–O–Fe–Pt/SiC membranes-coated DPF and compare it with other catalysts. However, our main objective was to develop the catalytic activity of SiC which has been demonstrated through the preparation of Ce–O–Fe–Pt/SiC membranes-coated DPF from reverse AHPCS-based microemulsion. Further works are under investigation to compare the present results with the same compositions in form of powders, with the mixed oxide and metallic phases (without SiC) as well as with CeO<sub>2</sub>/SiC, Ce–O–Pt/SiC membranes to better estimate the performance of the membranes and identify the role of each oxide phase for developing the catalytic properties of SiC. This was not the subject of the present paper and this will be published separately.

#### 3.4.2. Soot Combustion

The catalytic activity of soot oxidation over the Ce–O–Fe–Pt/SiC membrane-coated DPF is evaluated and is shown in Fig. 13 and

compare to the SiC material. The variations of the pressure drop and of the PN emissions are shown on the Fig. 13a and c. During the first minutes of the soot loading, the filtration efficiency is poor since the surface pores of walls are being filled up with soot. This resulted in an abrupt pressure drop ( $\Delta P$ ). The presence of the membrane slightly decreases the PN emission without increasing the pressure drop. After around 9 min, the surface pores are filled and a quite effective filtering is ensured by the soot cake, leading to a lower ramp increase of the pressure drop. It should be mentioned that performances are in general lower than that of CeO<sub>2</sub>-based catalyst powders for soot combustion [65]. However, for practical purposes, the catalytically active component should be supported as a film on a structured substrate, thus allowing simultaneous soot filtration and combustion which is not the case for powders. Furthermore, it should be noticed that SiC was active although a very low quantity of catalyst precursors was used. This means that there is a soot-to-catalyst contact. Compared with SiC DPF coated with oxide phases (not dispersed in a SiC membrane)

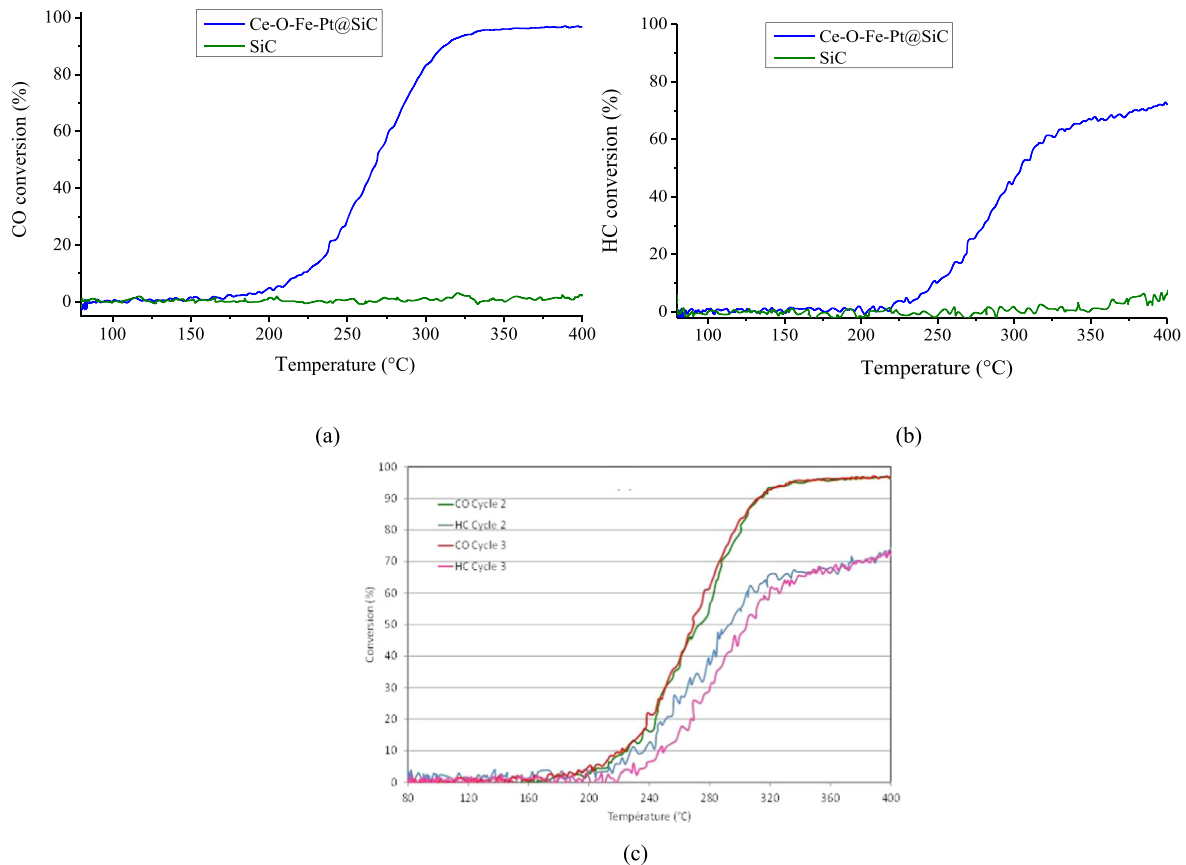


**Fig. 12.** (a) CO conversion rate and (b) HC conversion rate as a function of reaction temperature for the SiC10 membrane-coated DPF and the Ce–O–Fe–Pt/SiC membranes supported on DPF. (c) CO conversion rate and HC conversion rate as a function of reaction temperature for the Ce–O–Fe–Pt/SiC membranes supported on DPF after three cycles.

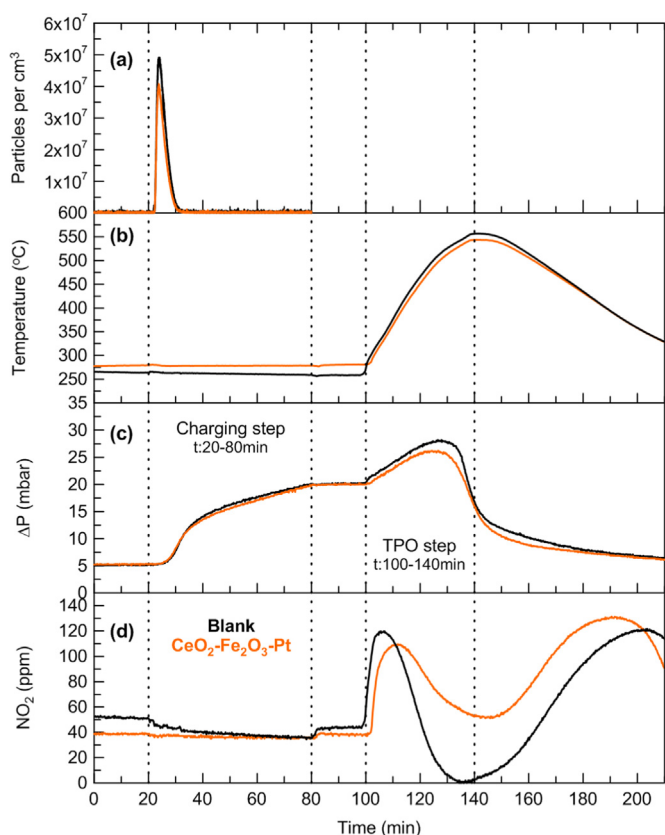


**Fig. 13.** Loading and unloading cycles for the coated samples with (a) amount of particles exhaust during the loading (b) temperature variation (c) evolution of the pressure drop and (d)  $\text{NO}_2$  concentration variation.

[64], the performances are similar. These observations confirm the interest of our approach whereas we expect higher durability.

The TPO experiment starts after around 100 min on stream. The initial pressure drop increases with temperature is due to the gas viscosity enhancement. When the soot cake burns off leading to a decrease in the pressure drop. One can observe that the presence of the catalyst on the membrane allows burning the soot at a lower temperature: 486 °C instead of 518 °C without any catalytic phases. In addition, as shown in Fig. 13c, the Ce–O–Fe–Pt/SiC membranes-coated DPF allowed getting the lowest pressure drop (26.1 mbar in comparison to 28.0 (without catalytic phases)). During TPO, the variation of the  $\text{NO}_2$  concentration with temperature follows an inverted volcano curve. The minimum in the  $\text{NO}_2$  concentration occurs in the same temperature range of the pressure drop decrease. This underlines that soot is mainly oxidized with  $\text{NO}_2$ .  $\text{NO}_2$  is catalytically produced by the oxidation of NO in the mini-DOC and also in the catalyzed mini-DPF. Our result emphasizes that the production of  $\text{NO}_2$  is higher in the catalyzed DPFs, explaining the better catalytic behaviors for soot oxidation.

These results demonstrated the interest of our approach to develop the catalytic activity of SiC materials. This approach is interesting for not only use on DPF but also other catalytic reactions.

#### 4. Conclusion

In the present paper, we have demonstrated that one of the most desirable ways for increasing the filtration efficiency (future emission standards), durability and catalytic activity of DPF was to use an additional fine porous filtration SiC-based membrane

(~150 nm in thickness) deposited on the filter wall using allylhydridopolycarbosilane (AHPCS) as a SiC precursor. In the first part of the present study, thin SiC membranes were prepared by dip-coating DPF in AHPCS solutions (10 vol% in THF) then pyrolyzed at 1000 °C under argon to reduce the porosity and the pore diameter without affecting the back pressure of the filter. It should be mentioned that the membrane provided a better durability to the DPF as demonstrated by high temperature TGA and soot loading experiments. Similar results have been obtained using a commercially-available polycarbosiloxane (Si–C–O precursor). To develop the catalytic activity of the membrane, we investigated in the second part of the present paper a reverse AHPCS-based microemulsion and, as a preliminary study, we developed Ce–O–Fe–Pt/SiC membrane coated DPF after dip-coating and pyrolysis under argon at 1000 °C. These materials have been successfully tested for CO/HC oxidation and soot combustion. Ce–O–Fe–Pt/SiC membrane coated DPF showed an activity for CO conversion reaching a light-off temperature  $T_{50}=270$  °C and the presence of the catalytic phase allowed burning soot 30 °C below the SiC membrane. Although the initial capital cost of general polymer-derived ceramics is above than that of more conventional powder technologies; the polymer-derived ceramic membranes reported here are durable, safe (the catalyst phase is confined in the SiC membrane with no possibility to be removed) and the impregnation of DPF is probably more efficient than a washcoat for example. Furthermore, only 10 vol% of AHPCS are used to prepare the membranes, which is clearly economically advantageous. This proves the interest of our approach in pursuit of practical implementation of Si-based ceramic nanocomposites in environmental and green technologies.

#### Acknowledgment

The authors gratefully acknowledge the financial contribution from Ademe (Agence De l'Environnement et de la Maîtrise de l'Energie) (N°TEZ10-22) and G. Blanchard from PSA Peugeot-Citroen for the scientific discussions which were beneficial for the present study. The authors also acknowledge the LabEx CheMISyst (2012-2015) from University of Montpellier (ANR-10-LABX-05-01) (Scientific council call for proposal 2012). Prof. C. Balan acknowledges the financial support from the Grants of the Ministry of National Education, Romania, CNCS-UEFISCDI: PN-II-ID-PCE-2012-4-0245.

#### Appendix A. Supplementary material

Supplementary data associated with this article can be found in the online version at <http://dx.doi.org/10.1016/j.memsci.2015.12.015>.

#### References

- [1] I.F.J. Vankelecom, Polymeric membranes in catalytic reactors, *Chem. Rev.* **102** (2002) 3779–3810.
- [2] (a) Y. Iwamoto, H. Kawamoto, In science and technology trends, *Q. Rep.* **32** (2009) 42–59;  
(b) A.G. Fane, R. Wang, M.X. Hu, Synthetic membranes for water purification: status and future, *Angew. Chem. Int. Ed.* **54** (2015) 3368–3386.
- [3] B. Elyassi, M. Sahimi, T.T. Tsotsis, Inorganic Membranes. Encyclopedia of Chemical Processing, in: Lee (Ed.), Taylor & Francis Group, 2009, pp. 1–16 (LLC, Sunggyu (K.B.)).
- [4] R.O. McClellan, T.W. Hesterberg, J.C. Wall, Evaluation of carcinogenic hazard of diesel engine exhaust needs to consider revolutionary changes in diesel technology, *Regul. Toxicol. Pharmacol.* **63** (2012) 225–258.
- [5] A. Pronk, J. Coble, P.A. Stewart, Occupational exposure to Diesel engine

- exhaust: a literature review, *J. Expo. Sci. Environ. Epidemiol.* 19 (2009) 443–457.
- [6] L. Le Grand Les entreprises, acteurs de la recherche et de l'innovation – Le système Filtre à Particules (FAP<sup>®</sup>): Une rupture technologique au service de l'environnement. Entretien PSA Peugeot Citroën. (in french), 2005.
- [7] D. Fino, Diesel emission control: catalytic filters for particulate removal, *Sci. Technol. Adv. Mater.* 8 (2007) 93–100.
- [8] B.A.A.L. Van Setten, M. Makkee, J.A. Moulijn, Science and technology of catalytic diesel particles oxidation, *Catal. Rev. Sci. Eng.* 43 (2001) 489–564.
- [9] K. Pattas, Z. Samaras, D. Sherwood, K. Umehara, C. Cantiani Aguerre, O. Chariol Ph Barthe, J. Lemaire, Cordierite filter durability with cerium fuel additive: 100,000 km of revenue service in athens. SAE Technical Paper Series, 1992, 920363–920377.
- [10] G. Blanchard, C. Colignon, C. Griad, C. Rigaudeau, O. Salvat, T. Seguelong, Passenger car series application of a new diesel particulate filter system using a new ceria-based fuel-borne catalyst: From the Engine Test Bench to European Vehicle Certification. SAE Technical Paper Series, 2002, pp. 2781–2794.
- [11] L. Rocher, T. Seguelong, V. Harle, M. Lallemand, M. Pudlarz, M. Macduff, New generation fuel borne catalyst for reliable DPF operation in globally diverse fuels. SAE Technical Paper Series, 2011, pp. 297–309.
- [12] S. Biamino, P. Fino, N. Russo, C. Badini, Catalyzed traps for diesel soot abatement: In situ processing and deposition of perovskite catalyst, *Appl. Catal. B: Environ.* 61 (2005) 297–305.
- [13] C.A. Neyertz, E.E. Miro, M. A. Querin, K/CeO<sub>2</sub> catalysts supported on cordierite monoliths: Diesel soot combustion study, *Chem. Eng. J.* 181–182 (2012) 93–102.
- [14] M.E. Galvez, S. Ascaso, I. Tobias, R. Moliner, M.J. Lazaro, Catalytic filters for the simultaneous removal of soot and NO<sub>x</sub>: Influence of the alumina precursor on monolith washing and catalytic activity, *Catal. Today* 191 (2012) 96–105.
- [15] E.D. Banus, V.G. Milt, E.E. Miro, M.A. Ulla, Catalytic coating synthesized onto cordierite monolith walls. Its application to Diesel soot combustion, *Appl. Catal. B: Environ.* 132–133 (2013) 479–486.
- [16] E.E. Miro, F. Ravelli, M.A. Ulla, L.M. Cornaglia, C.A. Querin, Catalytic combustion of diesel soot on Co,K supported catalysts, *Catal. Today* 53 (1999) 631–638.
- [17] A. Trovarelli, Catalytic properties of ceria and CeO<sub>2</sub>-containing materials, *Catal. Rev. Sci. Eng.* 38 (1996) 439–520.
- [18] A. Bueno-López, Diesel soot combustion ceria catalysts, *Appl. Catal. B: Environ.* 146 (2014) 1–11.
- [19] Q. Shen, M. Wu, H. Wang, C. He, Z. Hao, W. Wei, Y. Sun, Facile synthesis of catalytically active CeO<sub>2</sub> for soot combustion, *Catal. Sci. Technol.* 5 (2015) 1941–1952.
- [20] H. Muroyama, H. Asajima, S. Hano, T. Matsui, K. Eguchi, Effect of an additive in a CeO<sub>2</sub>-based oxide on catalytic soot combustion, *Appl. Catal. A: Gen.* 489 (2015) 235–240.
- [21] A.G. Acheson, British Patent No. 17911, 1892.
- [22] W.F. Knippenberg, Growth phenomena in silicon carbide. Philips Research Reports 18. Edited by the research laboratory of N. V. Philips Gloeilampenfabriken, Eindhoven, Netherlands, 1963, pp. 161–274.
- [23] N. Yoshida, S. Terazawa, K. Hayashi, T. Hamaguchi, H. Natsuhara, S. Nonomura, A narrow process window for the preparation of polytypes of microcrystalline silicon carbide thin films by hot-wire CVD method, *J. Non-Cryst. Solids* 358 (2012) 1987–1989.
- [24] R. Hashimoto, A. Ito, T. Goto, Effect of deposition atmosphere on the phase composition and microstructure of silicon carbide films prepared by laser chemical vapour deposition, *Ceram. Int.* 41 (2015) 6898–6904.
- [25] M.-C. Bechelany, V. Proust, C. Gervais, R. Ghisleny, S. Bernard, P. Miele, In-situ controlled growth of titanium nitride in amorphous silicon nitride: a general route toward bulk non-oxide nitride nanocomposites with very high hardness, *Adv. Mater.* 26 (2014) 6548–6553.
- [26] G. Mera, M. Gallei, S. Bernard, E. Ionescu, Ceramic nanocomposites from tailor-made preceramic polymers, *Nanomaterials* 5 (2015) 468–540.
- [27] C. Zhou, X. Gao, Y. Xu, G. Buntkowsky, Y. Ikuhara, R. Riedel, E. Ionescu, Synthesis and high-temperature evolution of single-phase amorphous Si–Hf–N ceramics, *J. Eur. Ceram. Soc.* 35 (2015) 2007–2015.
- [28] Z. Yu, L. Yang, H. Min, P. Zhang, A. Liu, R. Riedel, High-ceramic-yield precursor to SiC-based ceramic: a hyperbranched polytitaniumcarbosilane bearing self-catalyzing units, *J. Eur. Ceram. Soc.* 35 (2015) 851–858.
- [29] J. Kaspar, C. Terzioglu, E. Ionescu, M. Graczyk-Zajac, S. Hapis, H.-J. Kleebe, R. Riedel, Stable SiOC/Sn nanocomposite anodes for lithium-ion batteries with outstanding cycling stability, *Adv. Funct. Mater.* 24 (2014) 4097–4104.
- [30] Q. Wen, Y. Xu, B. Xu, C. Fasel, O. Guillon, G. Buntkowsky, Z. Yu, R. Riedel, E. Ionescu, Single-source-precursor synthesis of dense SiC/HfC<sub>1-x</sub>-based ultrahigh-temperature ceramic nanocomposite, *Nanoscale* 6 (2014) 13678–13689.
- [31] M. Zaheer, J. Hermannsdörfer, W.P. Kretschmer, G. Motz, R. Kempe, Robust Heterogeneous Nickel Catalysts with Tailored Porosity for the selective hydrogenolysis of aryl ethers, *Chem. Cat. Chem.* 6 (2014) 91–95.
- [32] S. Bernard, P. Miele, Polymer-Derived Boron Nitride: a review on the Chemistry, shaping and ceramic conversion of borazine derivatives, *Materials* 7 (2014) 7436–7459.
- [33] S. Bernard, P. Miele, Nanostructured and architected boron nitride, *Mater. Today* 17 (2014) 443–450.
- [34] P. Colombo, G. Mera, R. Riedel, G.D. Soraru, Polymer-derived ceramics: 40 years of research and innovation in advanced ceramics, *J. Am. Ceram. Soc.* 93 (2010) 1805–1837.
- [35] L. Gottardo, S. Bernard, C. Gervais, M. Weinmann, P. Miele, Study of the intermediate pyrolysis steps and mechanism identification of polymer-derived SiBCN ceramics, *J. Mater. Chem.* 22 (2012) 17923–17933.
- [36] L. Gottardo, S. Bernard, C. Gervais, K. Inzenhofer, G. Motz, M. Weinmann, C. Balan, P. Miele, Chemistry, structure and processability of boron-modified polysilazanes as tailored precursors of ceramic fibers, *J. Mater. Chem.* 22 (2012) 7739–7750.
- [37] O. Majoulet, J.G. Alauzun, L. Gottardo, C. Gervais, M.E. Schuster, S. Bernard, P. Miele Ordered, Mesoporous silicoboron carbonitride ceramics from boron-modified polysilazanes: polymer synthesis, *Process. Prop. Microporous Mesoporous Mater.* 140 (2011) 40–50.
- [38] L. Meng, X. Zhang, Y. Tang, K. Su, J. Kong, Hierarchically porous silicon-carbon-nitrogen hybrid materials towards highly efficient and selective adsorption of organic dyes, *Sci. Rep.* 5 (2015) 7910–7925.
- [39] (a) O. Majoulet, C. Salameh, M.E. Schuster, U.B. Demirci, Y. Sugahara, S. Bernard, P. Miele, Synthesis of periodic mesoporous silicon-aluminum-carbon-nitrogen frameworks surface-decorated with Pt nanoparticles, *Chem. Mater.* 25 (2013) 3957–3970;
- (b) C. Salameh, A. Bruma, S. Malo, U.B. Demirci, P. Miele, S. Bernard, Monodisperse platinum nanoparticles supported on highly ordered mesoporous silicon nitride nanoblocks: superior catalytic activity for hydrogen generation from sodium borohydride, *RSC Adv.* 5 (2015) 58943–58951.
- [40] L. David, S. Bernard, C. Gervais, P. Miele, G. Singh, High capacity and rate capability of SiCN/BN nanosheet composite as Li-ion battery electrode, *J. Phys. Chem. C* 119 (2015) 2783–2791.
- [41] P. Colombo, T.E. Paulson, C.G. Pantano, Atmosphere effects in the processing of silicon carbide and silicon oxycarbide, *Thin Films Coat. J. Sol-Gel Sci. Technol.* 2 (1994) 601–604.
- [42] M.R. Mucalo, N.B. Milestone, I.C. Viclridge, M.V. Swain, Preparation of ceramic coatings from pre-ceramic precursors. Part I SiC and “Si<sub>3</sub>N<sub>4</sub>/Si<sub>2</sub>N<sub>2</sub>O” coatings on alumina substrates, *J. Mater. Sci.* 29 (1994) 4487–4499.
- [43] M.R. Mucalo, N.B. Milestone, Preparation of ceramic coatings from pre-ceramic precursors. Part II SiC on metal substrates, *J. Mater. Sci.* 29 (1994) 5934–5946.
- [44] P. Colombo, T.E. Paulson, C.G. Pantano, Synthesis of silicon carbide thin films with Polycarbosilane (PCS), *J. Am. Ceram. Soc.* 80 (1997) 2333–2340.
- [45] T.J. Cross, R. Raj, S.V. Prasad, D.R. Tallant, Synthesis and tribological behavior of silicon oxycarbonitride thin films derived from poly(Urea)methyl vinyl silazane, *Int. J. Appl. Ceram. Technol.* 3 (2006) 113–126.
- [46] M. Günthner, T. Kraus, A. Dierdorf, D. Decker, W. Krenkel, G. Motz, Advanced coatings on the basis of Si(C)N precursors for protection of steel against oxidation, *J. Eur. Ceram. Soc.* 29 (2009) 2061–2068.
- [47] M. Günthner, K. Wang, R.K. Bordia, G. Motz, Conversion behaviour and resulting mechanical properties of polysilazane-based coatings, *J. Eur. Ceram. Soc.* 32 (2012) 1883–1892.
- [48] Z. Xie, S. Cao, J. Wang, X. Yan, S. Bernard, P. Miele, Engineering of silicon-based ceramic fibers: novel SiTaC(O) ceramic fibers prepared from polytantalosilane, *Mater. Sci. Eng. A* 527 (2010) 7086–7091.
- [49] E. Kockrick, P. Krawiec, U. Petasch, H.-P. Martin, M. Herrmann, S. Kaskel, Porous CeO<sub>2</sub>/SiC nanocomposites prepared from reverse polycarbosilane-based microemulsions, *Chem. Mater.* 20 (2008) 77–83.
- [50] E. Kockrick, R. Frind, M. Rose, U. Petasch, W. Böhlmann, D. Geiger, M. Herrmann, S. Kaskel, Platinum induced crosslinking of polycarbosilanes for the formation of highly porous CeO<sub>2</sub>/silicon oxycarbide catalysts, *J. Mater. Chem.* 19 (2009) 1543–1553.
- [51] C. Hoffmann, T. Biemelt, M.R. Lohe, M.H. Rummeli, S. Kaskel, Nanoporous and highly active silicon carbide supported CeO<sub>2</sub>-catalysts for the methane oxidation reaction, *Small* 10 (2014) 316–322.
- [52] R.J. Ciora, B. Fayyaz, P.K.T. Liu, V. Suwanmethanon, R. Mallada, M. Sashimi, T. T. Tsotsis, Preparation and reactive applications of nanoporous silicon carbide membranes, *Chem. Eng. Sci.* 59 (2004) 4957–4965.
- [53] V.V. Gulians, M.A. Carreon, Y.S. Lin, Ordered mesoporous and macroporous inorganic films and membranes, *J. Membr. Sci.* 235 (2004) 53–72.
- [54] B. Elyassi, M. Sahimi, T.T. Tsotsis, A novel sacrificial interlayer-based method for the preparation of silicon carbide membranes, *J. Membr. Sci.* 316 (2008) 73–79.
- [55] W. Deng, X. Yu, M. Sahimi, T.T. Tsotsis, Highly permeable porous silicon carbide support tubes for the preparation of nanoporous inorganic membranes, *J. Membr. Sci.* 451 (2014) 192–204.
- [56] B. Elyassi, M. Sahimi, T.T. Tsotsis, Silicon carbide membranes for gas separation applications, *J. Membr. Sci.* 288 (2007) 290–297.
- [57] R. Riedel, G. Mera, R. Hauser, A. Klönczynski, Silicon based polymer derived ceramics: synthesis properties and applications – A review, *J. Ceram. Soc. Jpn.* 114 (2006) 425–444.
- [58] C.K. Whitmarsh, L.V. Interrante, Carbosilane polymer precursors to silicon carbide ceramics, U.S. Patent No. 5, October 6, 1992, pp. 153–295.
- [59] Starfire Systems, Inc., 877 25th St., Watervliet, NY, 12189.
- [60] Z. Gu, X. Sang, H. Wang, K. Li, Structure and catalytic property of CeO<sub>2</sub>-ZrO<sub>2</sub>-Fe<sub>2</sub>O<sub>3</sub> mixed oxide catalysts for diesel soot combustion: effect of preparation method, *J. Rare Earths* 32 (2014) 817–823.
- [61] & Z.L. Zhang, D. Han, S.J. Wei, Y.X. Zhang, Determination of active sites densities and mechanisms for soot combustion with O<sub>2</sub> on Fe-doped CeO<sub>2</sub> mixed oxides, *J. Catal.* 276 (2010) 16–23.
- [62] & Q. Li, X. Wang, Y. Xin, Z. Zhang, Y. Zhang, C. Hao, M. Meng, L. Zheng, L. A. Zheng, unified intermediate and mechanism for soot combustion on potassium-supported oxides, *Sci. Rep.* 4 (2014) 4725–4730.
- [63] Z. Gu, K. Li, S. Qing, X. Zhu, Y. Wei, Y. Li, H. Wang, Enhanced reducibility and redox stability of Fe<sub>2</sub>O<sub>3</sub> in the presence of CeO<sub>2</sub> nanoparticle, *RSC Adv.* 4

- (1958) 47191–47199.
- [64] S. Quilos-Díaz, J. Gimenez-Manogil, A. Garcia-Gareea, Catalytic performance of  $\text{CuO/Ce}_{0.8}\text{Zr}_{0.2}\text{O}_2$  loaded onto SiC-DPF in NO<sub>x</sub>-assisted combustion of diesel soot, *RSC Adv.* 5 (2015) 17018–17029.
- [65] L.F. Nascimento, R.F. Martins, R.F. Silva, O.A. Serra, Catalytic combustion of soot over ceria-zinc mixed oxides catalysts supported onto cordierite, *J. Env. Sci.* 26 (2014) 694–701.
- [66] X.L. Lizarraga, S. Souentie, A. Boreave, C. George, B.D. Anna, P. Vernoux, Effect of diesel oxidation catalysts on the diesel particulate filter regeneration process, *Environ. Sci. Technol.* 45 (2011) 10591–10597.
- [67] S. Yajima, J. Hayashi, M. Omori, Continuous silicon carbide fiber of high tensile strength, *Chem. Lett.* 4 (1975) 931–934.
- [68] S. Yajima, Y. Hasegawa, J. Hayashi, M. Imura, Synthesis of continuous silicon carbide fiber with high tensile strength, *J. Mater. Sci.* 13 (1978) 2569–2576.
- [69] S. Yajima, Y. Hasegawa, M. Imura, Synthesis of continuous silicon carbide fiber part 2 conversion of polycarbosiiane fiber into silicon carbide fibers, *J. Mater. Sci.* 15 (1980) 720–728.
- [70] S. Duperrier, A. Calin, S. Bernard, C. Balan, P. Miele, Rheological behaviour of Poly[(B-alkylamino)borazine] in a fiber spinning process, *Soft. Mater.* 4 (2006) 123–142.
- [71] S. Duperrier, S. Bernard, A. Calin, C. Sigala, R. Chiriac, P. Miele, C. Balan, Design of a series of preceramic B-tri(methylamino)borazine-based polymers as fiber precursors: shear rheology investigations, *Macromolecules* 40 (2007) 1028–1034.
- [72] T. Ouyang, L. Gottardo, S. Bernard, C. Balan, P. Miele, Tuning of the viscoelastic properties of melt-spinnable boron- and silicon-based preceramic polymers, *J. Appl. Polym. Sci.* 128 (2013) 248–257.
- [73] J.D. Baird, J. Taylor, Reaction between silica and carbon and the activity of silica in slag solution, *Trans. Faraday Soc.* 54 (1958) 526–539.
- [74] G.S. Bibbo, P.M. Benson, C.G. Pantano, Effect of carbon monoxide partial pressure on the high-temperature decomposition of NICALON fibers, *J. Mater. Sci.* 26 (1991) 5075–5080.